Journal of Magnetic Resonance 327 (2021) 106980

Contents lists available at ScienceDirect

Journal of Magnetic Resonance

journal homepage: www.elsevier.com/locate/jmr

Describing angular momentum conventions in circularly polarized optically pumped NMR in GaAs and CdTe

Michael E. West, Erika L. Sesti, Matthew. M. Willmering, Dustin D. Wheeler, Zayd L. Ma, Sophia E. Hayes

Department of Chemistry, Washington University in St. Louis, St. Louis, MO 63130, United States

ARTICLE INFO

Article history:
Received 3 March 2021
Revised 8 April 2021
Accepted 9 April 2021
Available online 20 April 2021

Keywords:
GaAs
CdTe
OPNMR

ABSTRACT

The physical phenomena governing hyperpolarization through optical pumping of conduction electrons continue to be explored in multiple semiconductor systems. One early finding has been the asymmetry between the optically pumped nuclear magnetic resonance (OPNMR) signals when generated by different circular polarizations (*i.e.*, light helicities). Because these resonances are asymmetric, the midpoint between the signals prepared with each of the two circular polarizations is either a positive or negative value, termed an "offset" that is representative of an optical Overhauser enhancement. Both negative offsets (in GaAs) and positive offsets (in CdTe) have been observed. The origins of these offsets in semiconductors are believed to arise from thermalized electrons; however, to the best of our knowledge, no study has systematically tested this hypothesis. To that end, we have adopted two configurations for OPNMR experiments—one in which the Poynting vector of the laser light and magnetic field are parallel, and one in which they are antiparallel, while other experimental conditions are kept the same. We find that the OPNMR signal response to a fixed helicity of light depends on the experimental configuration, and this configuration needs to be accounted for in order to properly describe the OPNMR results. Further, studying the offsets as a function of field strength shows that the optical Overhauser enhancement (the offset) increases in magnitude with field strength. Finally, by describing all angular momentum and phasing conventions unambiguously, we are able to determine that the absorptively-phased appearance of ^{113}Cd (and ^{125}Te) OPNMR in CdTe is a consequence of the sign of the nuclear gyromagnetic ratios for these isotopes.

1. Introduction

Orientation of electron spins and their hyperfine coupling to nuclear spins is the underpinning of a wide range of emerging techniques in magnetic resonance and magneto-optics [1–6]. These couplings are of interest in candidate systems for quantum computing, notably in nitrogen vacancy (NV) centers in diamonds [3,7,8], trapped ions [9–11], semiconductors [12–15], and quantum dots [16–18]. Because these diverse systems converge onto similar topics, there is a need to unify nomenclatures and conventions among these many topical areas.

Optical pumping (OP) in nuclear magnetic resonance (NMR) spectroscopy is an ideal system in which to explore some of these conventions. NMR benefits from underlying definitions, where the quantization axis (and therefore orientation) of spin states depends only on the orientation of the external magnetic field, $\boldsymbol{B}_0$. Nevertheless, in many reports of magnetic resonance experiments, the orientation of $\boldsymbol{B}_0$ in the laboratory is omitted, or sometimes not known because the orientation is not germane to the NMR experiment. This absence brings up challenges when addressing physical phenomena observed in hyperpolarized NMR involving optics and magnetic fields, as omission of a reference frame may lead to different interpretations.

For comparison, in NV center experiments, the states are (often) instead quantized based on the axis parallel to the nitrogen-vacancy "bond" instead of an external magnetic field. In experiments where NV axes are not parallel to $\boldsymbol{B}_0$, the absorption rules become complicated because the circularly polarized light becomes elliptical in the NV frame [19–21].

The intent of this work is to demonstrate how different experimental configurations impact measurements and conclusions in hyperpolarized systems of semiconductors. Additionally, we believe the principles demonstrated here—specifically the explicit stating of the experimental configuration and the determination of the resulting quantization axis based on conventions—should be adopted by other hyperpolarization scheme reports. These would facilitate strong cross-readability between disciplines, as well as minimize ambiguity.

E-mail address: hayes@wustl.edu (S.E. Hayes)

https://doi.org/10.1016/j.jmr.2021.106980
1090-7807/

OPNMR hyperpolarization relies on optical pumping of conduction electrons in a semiconducting wafer with photons at or near the electronic band gap (E_g), shown on the left side of Fig. 1 (here, a direct gap species such as GaAs). For a detailed treatment, the photophysics of optical pumping in semiconductors is described extensively in multiple references[22–26]. At the top of the valence band and the bottom of the conduction band, the electronic states can be approximated as "atomic-like" energy levels with total angular momenta J = 3/2 and J = 1/2, respectively [24]. This is depicted on the right side of Fig. 1, where the lower energy levels represent the four m_J values for the states at the edge of the valence band, and the higher energy levels represent the two states at the edge of the conduction band. The Zeeman splitting of the m_J states (on the order of 10 μeV–100 μeV) are many orders of magnitude smaller than the band gap of the semiconductor (on the order of 1 eV), so the energy differences in m_J levels are not visible on this scale.

In practice, there are two possible experimental strategies for optical pumping with a colinear arrangement of magnetic field and light (*i.e.*, the Faraday configuration); the direction of the external magnetic field ($\boldsymbol{B}_0$) can either be parallel or antiparallel to the direction of light propagation ($\boldsymbol{k}$). We will depict these two configurations schematically in figures for ease of understanding experimental data, with a large blue arrow showing the direction of $\boldsymbol{B}_0$, and a wavy red arrow showing the direction of $\boldsymbol{k}$. This configuration has important implications for the data obtained, as we will show below.

OPNMR in semiconductors relies on the use of light to manipulate the electrons. Often, OPNMR experiments use circularly polarized light, meaning photons in the beam share the same value of angular momentum, either carrying + 1 or –1 in units of $\hbar$. Caution is needed when looking at the OPNMR and magneto-optical literature, as there are two common ways to define σ^+/σ^-. We use the definition that σ^+/σ^- light carries +1/–1 unit of angular momentum relative to the direction of the laser's propagation (the "Poynting vector," or $\boldsymbol{k}$). [1] When irradiated with photon energy at or above the band gap, electrons are promoted from the valence band to the conduction band, depicted as dashed red arrows in Fig. 1. In this example, $\boldsymbol{B}_0$ (blue arrow) is parallel to $\boldsymbol{k}$ (red wavy arrow), and m_J changes by +1 when σ^+ light is used.

A large conduction electron polarization is achieved by taking advantage of the different transition dipole strengths of the two allowed transitions when using circularly polarized light. A theoretical 3:1 transition probability ratio is expected due to the optical matrix elements[22] (depicted as the number of arrows on the right half of Fig. 1), leading to a population difference between the two conduction band electron states. Consequently, the instantaneous spin polarization in the conduction band, $\mathcal{P}_{OP}$, is expressed as the ratio of the difference in population over the sum:

$$\mathcal{P}_{OP} = \frac{N_\uparrow - N_\downarrow}{N_\uparrow + N_\downarrow} = \frac{1-3}{1+3} = -0.5 \qquad (1)$$

where $N_\uparrow$ is the number of conduction electrons pumped to the m_J = 1/2 state, and $N_\downarrow$ is the number of conduction electrons pumped to the $m_J = -1/2$ state. Depending on the helicity of light, $\mathcal{P}_{OP}$ takes on different signs. While we have found that this value has a photon energy dependence [25], we use this simplifying assumption for optical pumping just below E_g. In the example shown in Fig. 1, optical pumping results in a large, negative electron spin polarization of -50% (−0.5).

[1] σ^+/σ^- can also be defined based on the change in the spin quantum number of the electron during absorption, $\Delta m_J = \pm 1$. These are potentially conflicting definitions, therefore care is needed when comparing works between different publications (arising from different optical and magnetic field configurations) [19,27–31]

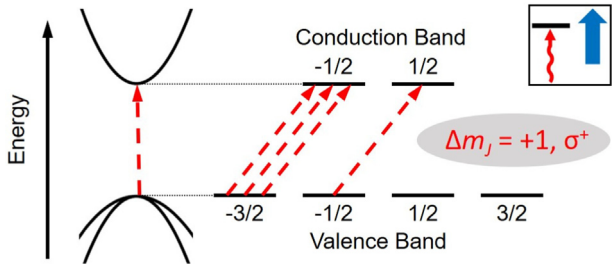

Fig. 1. Left: Diagram of the band structure of a direct gap semiconductor such as GaAs. Right: Schematic for bandedge states labelled with m_J values. Upon irradiation with circularly polarized light, valence electrons are excited to conduction band states with a change of m_J by +1 (in this example). The three dashed arrows connecting $|-3/2\rangle$ to $|-1/2\rangle$ states indicate this transition is three times more likely than the other transition. (Using the opposite helicity of light would change m_J states by −1, not shown). The inset schematic depicts both the direction of $\boldsymbol{B}_0$ (blue arrow) and laser Poynting vector (red wavy arrow). (For interpretation of the references to colour in this figure legend, the reader is referred to the web version of this article.)

Since the laser excites electrons into both the m_J = +1/2 and m_J = −1/2 states of the conduction electrons, 100% polarization is not achievable. It is worthwhile to note that using circularly polarized light as depicted in Fig. 1 (where $\Delta m_J = +1$), results in conduction electrons with a (net) negative polarization. Hyperfine coupling to nuclear spins then transfers the polarization from the hyperpolarized conduction band electronic m_J states to the nuclear m_I states. The hyperpolarized nuclei are then detected as an enhanced NMR signal (here negative, but with both positive and negative enhancements possible and dependent on the helicity of light) by application of a radio-frequency pulse sequence [24].

In magnetic resonance, we quantize the orientations of m_J and m_I states generally only in relation to the direction of $\boldsymbol{B}_0$ [32]. If $\boldsymbol{B}_0$ is reversed (or inverted from $\boldsymbol{B}_0\uparrow$ to $\boldsymbol{B}_0\downarrow$) in the laboratory frame, so are the orientations of the m states. Because m_J and m_I states describe the projection of quantized angular momentum on their quantization axis (on the $\boldsymbol{B}_0$ axis in this case), describing the absorption of a photon—which has its own quantization axis convention based on the direction of $\boldsymbol{k}$—can become complicated. Our study seeks to explain the consequences of NMR measurements when $\boldsymbol{k}$ and $\boldsymbol{B}_0$ are in different configurations. In the parallel configuration, as seen in Fig. 1, the two angular momentum conventions share the same reference frame. Here, a σ^+ photon would carry +1 unit of angular momentum with respect to $\boldsymbol{B}_0$, and therefore would change m_J by +1. However, in the antiparallel configuration, shown in Fig. 2, because the reference frames for the two

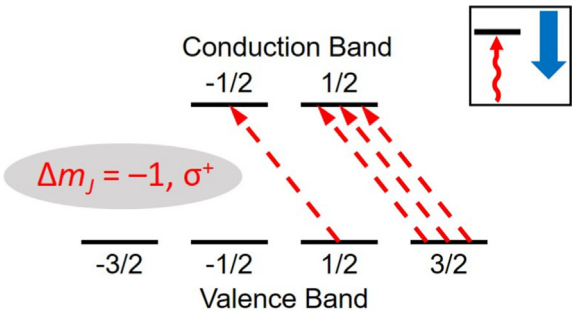

Fig. 2. Optical pumping diagram in the antiparallel configuration. When irradiated with σ^+ circularly polarized light, valence electrons are promoted to conduction band states with a change of m_J by −1. The inset schematic shows the direction of $\boldsymbol{B}_0$ (blue arrow) and laser Poynting vector (wavy red arrow). (For interpretation of the references to colour in this figure legend, the reader is referred to the web version of this article.)

angular momentum conventions are now inverted with respect to one another, a σ^+ photon would carry -1 unit with respect to $\boldsymbol{B}_0$, and therefore would change m_J by -1. For these reasons, the NMR phase and amplitude data for OPNMR and potentially other hyperpolarization schemes such as experiments in NV centers need to take into account these different configurations.

2. Experimental methods

A semi-insulating GaAs (si-GaAs) wafer from ITME, Warszawa (Ingot No. 2137, growth direction [100]) was used in the GaAs studies. The 400 μm thick wafer was cut into a rectangle of approximately 3 mm by 10 mm in order to fit in the NMR coil.

A homebuilt single-channel transmission line NMR probe was used in all the experiments [33,34]. In order to achieve sample temperatures of 6 ± 0.2 K, a Janis-200 Supertran continuous-flow cryostat was used; the temperature was monitored and controlled by a Lakeshore 340S temperature controller. The samples were mounted strain-free via Apiezon type N grease on a sapphire rod which acted as a heat sink.

The external magnetic field ($\boldsymbol{B}_0$) used for the first set of experiments was 4.697T (^{69}Ga Larmor frequency of 48.08 MHz) and aligned antiparallel to the incoming laser light. This field was reversed for a second set of experiments to the parallel configuration (bringing the superconducting magnet as close as possible to the same strength) at a field of 4.699 T (^{69}Ga Larmor frequency of 48.11 MHz).

Additional studies were performed on a high-resistivity, crystalline CdTe wafer in CdTe OPNMR profile studies. The 500 μm thick wafer was cut into a 2 mm by 4 mm rectangle. Experiments were performed in the parallel configuration in the 4.699 T external magnetic field (^{113}Cd Larmor frequency of 44.54MHz).

The pulse sequence used consisted of a saturating radio frequency (rf) pulse comb to ensure destruction of any net magnetization buildup between experiments, followed by a τ_L period of continuous-wave laser irradiation (10 min). The saturating comb and τ_L period were followed by a Bloch decay (single $\pi/2$ pulse) NMR experiment. A typical saturation train consisted of 50–100 small tip-angle pulses, with a 1 ms–2 ms delay in between. A single transient was recorded for all spectra unless otherwise noted. Notably, recycle delays are irrelevant here, because the laser establishes the spin polarization, instead of waiting for a time constant on the order of T_{1n}, the spin–lattice relaxation time constant. OPNMR signal only arises from the regions of the sample that are irradiated; T_{1n} is long enough that signal from thermal polarization in the entire sample during τ_L is negligible.

Laser irradiation was delivered by an 899–21 Coherent Ti-sapphire frequency-stabilized laser which was pumped with a 532 nm Spectra Physics Millenia Xs laser. The photon energy of the laser was monitored with an Ocean Optics HR-2000 spectrometer. A CVI Laser Optics zeroth-order quarter wave plate centered at 790 nm, placed in a rotational mount, was used to adjust the laser polarization from circular, to elliptical, to linear depending on its orientation. The waveplate was retained in the rotational mount for a given set of experiments, and the optical pathway was identical between the antiparallel and parallel versions of the experiments. At the sample, the beam was fixed to be a constant 100 mW of power with a beam diameter of 2 mm.

At the start of any set of experiments, once the sample reached a temperature of 6K, a ^{69}Ga NMR reference spectrum (the "Boltzmann" signal, also termed "thermal" herein) was recorded from the GaAs single crystal with a small tip angle pulse–acquire sequence, in the absence of any laser irradiation. Only a single transient was recorded. The NMR spectrum was phased absorptively, and that phase (the "system phase") was then applied to all other OPNMR spectra recorded subsequently on that day. Hence, any change in phase arises from coupling to the conduction electrons and their optically-oriented polarization.

3. Results and discussion

OPNMR signals have been studied with respect to the photon energy used for optical pumping. Examples of OPNMR "profiles" are shown in Fig. 3. These are plots of integrated NMR signal intensity, both positive and negative, as a function of the photon energy of the optical pumping light and, in particular, the helicity (circular

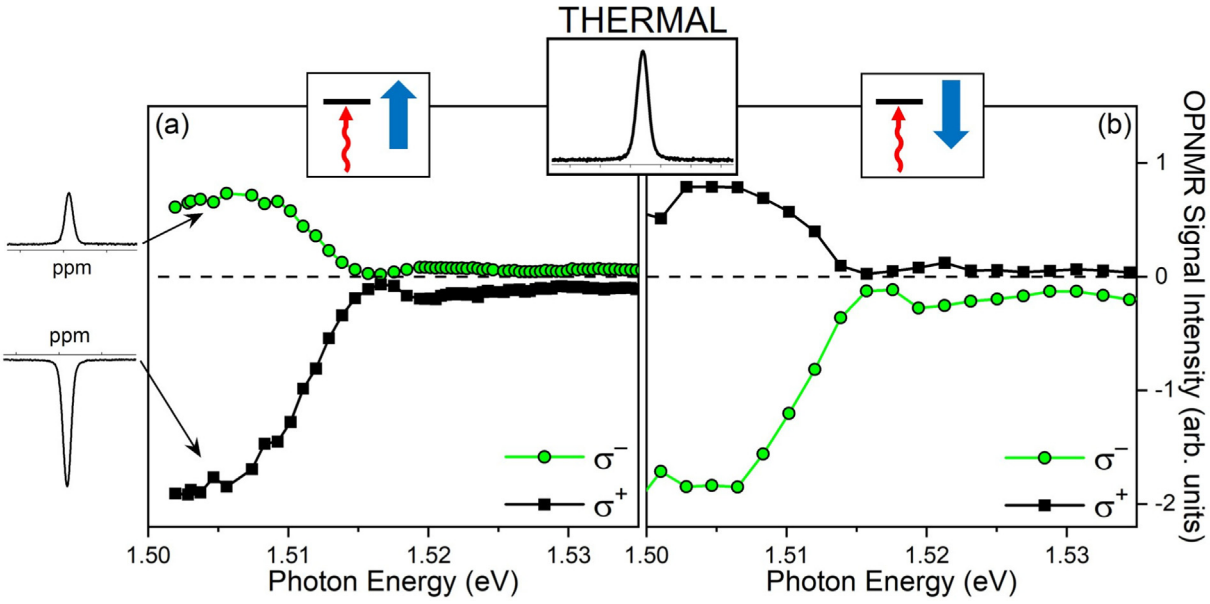

Fig. 3. OPNMR "profiles" as plots of integrated ^{69}Ga OPNMR spectra from semi-insulating single-crystal GaAs for two different light helicities. Black filled symbols are from σ^+ circularly polarized light, and green open symbols are from σ^- circularly polarized light. (a) ^{69}Ga OPNMR profile for the parallel orientation of the external magnetic field and the laser light's Poynting vector, and (b) for the antiparallel orientation of the external magnetic field and the Poynting vector. The ^{69}Ga NMR spectrum labeled "THERMAL" is the conventional ^{69}Ga NMR spectrum recorded at low temperature to set the phase for other experiments. (For interpretation of the references to colour in this figure legend, the reader is referred to the web version of this article.)

polarization) of the incoming laser light. To the far left of the figure are representative inset ^{69}Ga spectra that demonstrate these data appear as both "positive enhancements" (absorptively-phased) and "negative enhancements" (emissively-phased) spectra. OPNMR profiles exhibit a shape and detailed photon energy dependence that reflects a combination of both the penetration depth of the laser into the semiconductor sample [34–36], and details of the spin-split bandstructure arising from effects of the external magnetic field on the electrons of both the valence and conduction bands [26,37–40].

The reference thermal spectrum is shown in the middle inset of Fig. 3, and all data is phased with respect to it as outlined earlier. It is critical to note that this phasing convention does not necessarily impart knowledge of the orientation of nuclear spin angular momentum in the frame of reference of the laboratory. Irrespective of the sign of the gyromagnetic ratio, thermally polarized NMR signals (by a Boltzmann distribution) are phased absorptively. It is helpful to think of this spectrum's phase as independent of whichever experimental configuration is being used (parallel or antiparallel, as described previously).

Describing the phasing in such detail is important because many NMR researchers do not specify the direction of the field, $\boldsymbol{B}_0$, of their superconducting magnet in experimental reports, and for this reason, are unable to adequately describe the orientation of nuclear spin angular momentum with respect to the angular momentum of the photons. Here, we transform aspects of the experiment and the resulting physics into the reference frame of the magnetic field.

The OPNMR profile in Fig. 3a depicts data obtained in a parallel configuration of both the external magnetic field (the large blue arrow) and the Poynting vector of the laser light (the wavy red arrow). The ^{69}Ga OPNMR signal that results from using σ^- light (green open symbols) is positively enhanced (*i.e.*, absorptively-phased), whereas the signal from absorption of σ^+ light (black filled symbols) is negatively enhanced (emissively-phased), across the range of photon energies used for optical pumping of GaAs. Optical pumping with σ^+ laser light in the parallel configuration leads to more intense negatively-enhanced signals than the positively-enhanced signals from σ^-, as reported previously [4,25,33,34,38,39,41–47].

In this parallel configuration, σ^+ light produces a negative nuclear enhancement even though it introduces + 1 unit of angular momentum to the electron spins. This is because of the selection rules depicted in Fig. 1which produces a negative conduction electron spin polarization and therefore negative nuclear spin polarization. Likewise, σ^- light produces a positive enhancement by using equivalent and opposite selection rules. The asymmetry that is found between the relative intensities of two signals for a given photon energy originates from thermalization processes that are independent of the helicity of light used (described below).

We tested the outcome for the antiparallel configuration (between the external magnetic field and the laser Poynting vector), shown in 3b. To conduct this test with a superconducting (4.697 T) magnetic field, we discharged the magnet, and keeping all other aspects of the experiment the same, we re-charged the magnet with the opposite polarity at a nearly identical field strength (4.699 T). The thermal reference signal was phased absorptively, and the system phase was used for all subsequent experiments. The resulting OPNMR profile in Fig. 3b shows that σ^+ light (black filled symbols) now results in a positive enhancement, whereas σ^- (green open symbols) results in a negative enhancement—opposite in phase to the profile data in 3a—with the green open symbols following the direction of the $\boldsymbol{B}_0$ field. It is worth noting, the asymmetry is still present in this configuration, with larger negative enhancements than positive enhancements.

When the field direction is reversed, the two helicities of light "interchange" their effects. These observations are a consequence of the NMR phasing: for the parallel case, a σ^+ photon carries +1 unit of angular momentum relative to $\boldsymbol{B}_0$, whereas in the antiparallel case, a σ^+ photon carries −1 unit relative to $\boldsymbol{B}_0$. The signal asymmetry between pairs of σ^+/σ^- data points for a given photon energy can be expressed as the average between the two. This average value in Figs. 3a and 3b is negative, for both parallel and antiparallel configurations in contrast to the Boltzmann or "thermal" magnetization. A series of experiments were performed where the quarter-waveplate was rotated through multiple angles to produce elliptical and linearly-polarized light (π), similar to that shown previously for ^{69}Ga OPNMR [48]. Here, we are able to perform a similar experiment on light (polarization) dependence for both experimental configurations (parallel and antiparallel), and the OPNMR signal intensities are shown in Fig. 4 as a function of polarizer setting for parallel (blue solid symbols) and antiparallel (red open symbols) orientations. The experiments were performed at a fixed photon energy of 1.505 eV (≈ 9 meV below the GaAs excitonic absorption at 6 K). Vertical dashed lines are shown at polarizer settings of 20 degrees and 110 degrees, corresponding to σ^+ and σ^-, respectively. The signal intensity exhibits a sinusoidal relationship with the quarter-waveplate setting (expressed as an angle), and the asymmetry of the OPNMR signal is captured as an offset of the sine shapes (shown as the horizontal dashed line in the figure). The parallel and antiparallel configurations are 90° out of phase with respect to one another. These data are fit with offset sine waves and normalized so that the functions each have an amplitude of 1. The offsets are found to be −0.39 and −0.40 arb. units for the parallel and antiparallel orientations, respectively.

The origin of the observed nuclear hyperpolarization arises from cross-relaxation with the electronic spin polarization. A full description of the mechanism relies on accounting for nuclear spin diffusion and nuclear spin–lattice relaxation as a function of time [24]; however, when these contributions are ignored for simplicity, the steady-state *z*-component of nuclear spin polarization, assuming scalar relaxation, can be shown to have the form [49,50]:

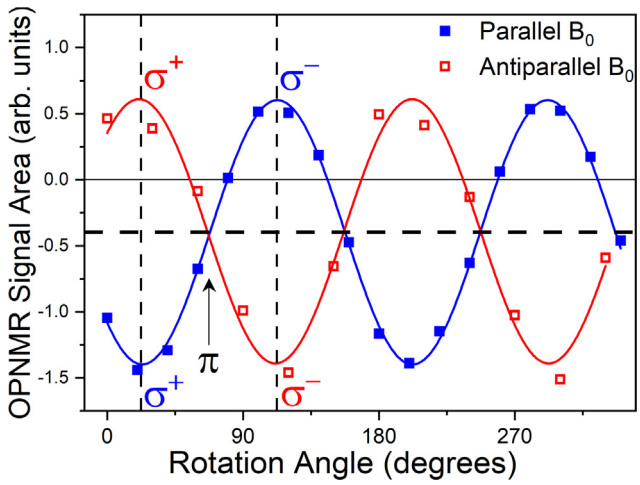

Fig. 4. OPNMR signal intensity as a function of rotation angle from optical mount markings of the quarter-wave plate for both magnetic field orientations. Data from the $\boldsymbol{B}_0$ field parallel to $\boldsymbol{k}$ are filled symbols, and the antiparallel configuration are open symbols. NMR signal intensities are normalized so that the amplitude of the fitted sine waves were 1 arb. units Offsets are –0.39 and –0.40 for parallel and antiparallel $\boldsymbol{B}_0$ orientations, respectively. Dashed vertical lines denote waveplate settings for σ^+ and σ^- polarizations, as indicated. The horizontal dashed line shows the midpoint of the sine functions, equivalent to the offset values for both. (For interpretation of the references to colour in this figure legend, the reader is referred to the web version of this article.)

$$\langle I_z \rangle = \frac{I(I+1)}{S(S+1)}(\langle S_z \rangle - S_0) \quad (2)$$

where $\langle S_z \rangle$ is the z-projection of the average electron spin polarization, I and S are the nuclear and electron quantum numbers, and S_0 is the conduction electron equilibrium spin polarization.

$\langle S_z \rangle$ can be shown to have the form [22,25,51]:

$$\langle S_z \rangle = \frac{T_{1e}}{T_{1e}+\tau_e} S_{opt} + \frac{\tau_e}{T_{1e}+\tau_e} S_0 \quad (3)$$

where T_{1e} is the electron spin lifetime, and τ_e is the electron recombination time. This equation is composed of two terms. The first term involves the creation of hyperpolarized, oriented conduction electrons via optical pumping, which is expressed as S_{opt}. The second term involves the population of spin-relaxed conduction electrons, S_0. The sign of the optically-generated spin polarization comes through the first term owing to optical orientation, whereas the second term arises from carriers occupying the states at (or just below) the conduction band edge which have spin-relaxed. This latter term (which is proportional to B_0/k_BT) therefore exhibits a dependence on the strength of the magnetic field, B_0.

S_0 is given by [24,50,51]:

$$S_0 = \frac{1}{2}\mathcal{P}_e = \frac{1}{2}\tanh\left(\frac{-g^*\mu_B B_0}{2k_B T}\right) \quad (4)$$

where μ_B is the Bohr magneton, k_B is the Boltzmann constant, T is the experimental temperature, B_0 is the strength of the magnetic field, and the value for g^* is given as the effective Landé g-factor [48,50,51], which we discuss below. (The minus sign in this equation originates from an early convention where the free electron g-factor was treated as a positive value, and other expressions for g are relative to that positive value [52,53]. Because of this early convention, when converting between expressions for g-factors and electron gyromagnetic ratios, γ_e, the expression must include a minus sign: $\gamma_e = -g\mu_B$ [50].)

We must consider the impacts of the orientations of Poynting vector ($\boldsymbol{k}$) and light helicity, with respect to the external magnetic field ($\boldsymbol{B}_0$), on the optically-generated electron spin polarization, S_{opt}. Noting that $\langle S_z \rangle$ divided by the electron spin quantum number, S = 1/2, equals polarization, $\mathcal{P}_{OP}$, we can capture the influence of these factors through these two expressions:

$$S_{opt(P)} = S \cdot \mathcal{P}_{OP}(\mp 1)_{\sigma^\pm} \quad \text{(parallel)} \quad (5)$$

$$S_{opt(AP)} = S \cdot \mathcal{P}_{OP}(\pm 1)_{\sigma^\pm} \quad \text{(antiparallel)} \quad (6)$$

where $\mathcal{P}_{OP}$ is assumed to be 0.5 (50%) at the band edge as discussed previously (Eq. (1)). In other words, the factor $(\mp 1)_{\sigma^\pm}$ for the sign of the enhancement is determined by using either σ^+ light (-1) or σ^- light ($+1$) for the parallel configuration, and the converse for antiparallel. Since the experimental configuration impacts the sign of the polarization, these two separate expressions are necessary.

When examining the data in Figs. 3 and 4, changing the helicity of light affects the nuclei so strongly that it can manipulate the orientation of nuclear spins, manifested as the enhancement (positive or negative) of the OPNMR signal. The asymmetry of the NMR signal intensities arises from contributions to the electron spin polarization from both thermal equilibrium conduction electron spin polarization and responses to the photon angular momenta of incoming light [25,41,48], described in Eqs. (2) and (3). The relative sizes of T_{1e} and τ_e play a role in determining the magnitude of this asymmetry; however, for the purposes of this discussion, we will focus only on the direction, or sign, of the asymmetry.

The sign of S_0 is invariant with respect to the helicity of light and the configuration of $\boldsymbol{k}$ with respect to $\boldsymbol{B}_0$; therefore, its effect on the electron polarization always has same sign. This convention puts the orientation of electrons into the reference frame of the magnet; hence, $\boldsymbol{B}_0$ will be expressed as a value, where using the magnitude removes potential sources of error if not considering the new reference frame. In fact, with an unpolarized or linearly polarized laser (S_{opt} = 0), Eqs. (2) and (3) would reduce to an optical Overhauser effect (OE), where nuclear enhancement is proportional to the equilibrium spin polarization of conduction electrons [54,55]. The optical OE is represented in Fig. 4 midway between sine curve peaks, which is depicted as the horizontal dashed line.

3.1. Field dependence

The waveplate rotation experiment was repeated at two other magnetic field strengths (3 T and 7 T). On the left side of Fig. 5, the waveplate rotation experiment in a 7 T field (in the parallel configuration) is depicted, showing a much larger offset (*i.e.*, asymmetry) compared to that of the 4.7 T experiments. Data were normalized using the same process as Fig. 4. On the right side of the figure, the values of the OPNMR signal offsets are plotted versus magnetic field. The offset becomes increasingly large and negative as B_0 increases; mathematically, as B_0 is increased, the magnitude of the offset is expected to increase according to Eq. (4), assuming T_{1e} and τ_e time constants do not change appreciably. (These data are not fit to a model because we would be unable to rigorously account for all field-dependent factors.) A larger offset corresponds to an increasing dominance of the second term in Eq. (3), which is directly proportional to B_0 [35].

3.2. OPNMR offsets in CdTe

CdTe has NMR-active nuclei (^{113}Cd and ^{125}Te) with negative nuclear gyromagnetic ratio values, $\gamma_{^{113}Cd}$ and $\gamma_{^{125}Te}$. We studied ^{113}Cd OPNMR of crystalline CdTe, and Leung and Michal studied ^{125}Te OPNMR of crystalline CdTe at cryogenic helium temperatures [56], both generating OPNMR profiles. (It is worthwhile to note that ^{111}Cd, ^{113}Cd and ^{123}Te were also studied, but at cryogenic nitrogen temperatures.) Notably, the parallel experimental configuration for ^{113}Cd OPNMR was used by us, whereas Leung and Michal used the antiparallel configuration for ^{125}Te studies. In both cases, a consistent treatment of sign and phasing leads to positive offsets (the average between the two signals for σ^+ and σ^- light, or positive OE enhancements). The ^{113}Cd OPNMR profile is shown in Fig. 6(a), and the ^{125}Te profile in Fig. 6(b). In the parallel configuration, σ^+ circularly polarized light leads to the most intense positive enhancement, whereas in the antiparallel configuration, σ^- leads to the most intense enhancement. Unlike the case for GaAs, the OPNMR signal does not change sign with a change in helicity.

The negative values for nuclear gyromagnetic ratios must be treated consistently with other data. By definition, the sign of equilibrium nuclear polarization, $\mathcal{P}_n$, is negative (anti-aligned with $\boldsymbol{B}_0$) when γ_n is negative. Consequently, any ^{113}Cd OPNMR spectrum that has a negative polarization will also be phased absorptively.

The findings for these semiconductors are shown in Table 1 that summarizes the various quantities and their signs under consideration in this study. We include results for ^{71}Ga OPNMR (data not shown). In past OPNMR literature, the Landé g-factor (g^*) used in Eq. (4) has been expressed to be that of the conduction electrons [24,25,48,51,57–62]. We note, CdTe has a negative g^* value like that of GaAs, measured by conduction electron spin resonance (CESR): -0.44 for GaAs [51], and −1.59 for CdTe [63].

We return to the initial experimental "assumption" used in OPNMR studies: that the thermal equilibrium signal (shown as "thermal" in the OPNMR figures) is phased absorptively, like that of a positive enhancement, irrespective of the experimental configuration of $\boldsymbol{B}_0$ and $\boldsymbol{k}$, whether parallel or antiparallel. This point is significant when considering the case of ^{113}Cd and ^{125}Te with their

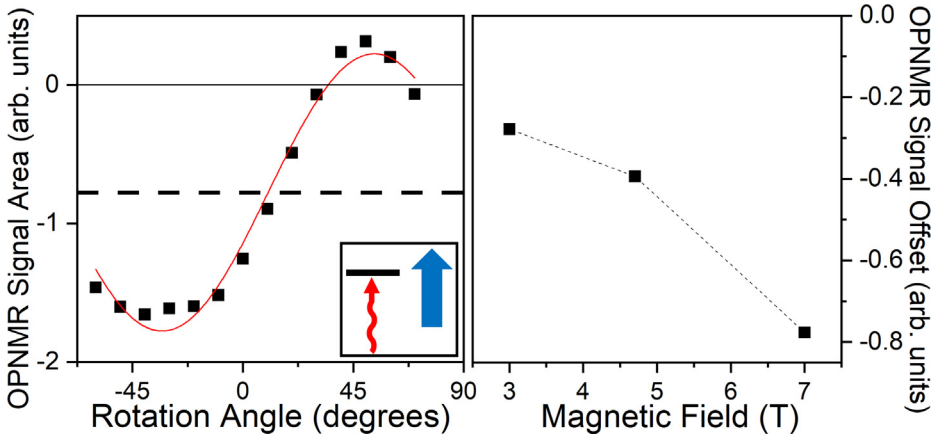

Fig. 5. (left) OPNMR signal intensity as a function of rotation angle of the quarter-waveplate in a 7 T field. The OPNMR experiment was performed in the parallel configuration. NMR signal intensities were normalized so that the amplitude of the fitted sine wave was 1 arb. units (right) Offset value as a function of magnitude of B_0.

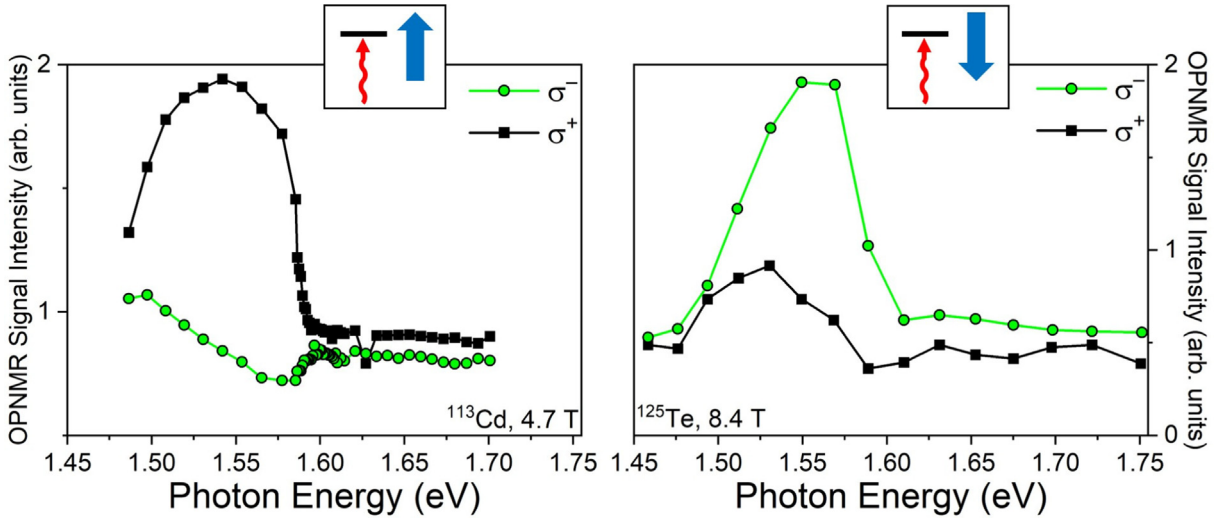

Fig. 6. OPNMR profiles as plots of integrated OPNMR spectra from semi-insulating single-crystal CdTe for two different light helicities. (a) ^{113}Cd OPNMR for the parallel configuration. Black filled symbols are from σ^+ light, and green open symbols are from σ^- light. (b) ^{125}Te OPNMR for the antiparallel configuration with the different symbols denoted in the legend. Inset images show representative spectra for the two helicities and in the absence of any laser irradiation "OFF". (For interpretation of the references to colour in this figure legend, the reader is referred to the web version of this article.)

Table 1
Predicted Signs of Optical OE Enhancements.

Sample	Nucleus Probed	Observed Optical OE (offset)	γ_n (10^7 rad/Ts)	Landé g^*
GaAs	^{69}Ga	–	+6.43	−0.44
	^{71}Ga	–	+8.17	−0.44
CdTe	^{113}Cd	+	−5.96	−1.59
	^{125}Te	+	−8.50	−1.59

negative gyromagnetic ratios. This positive OE offset arises from the NMR phasing, not from unique OPNMR phenomena for CdTe. Ultimately, when viewed with a phase chosen to make equilibrium signals appear absorptive, the sign of the offset is positive (parallel to the thermal equilibrium) if gamma is negative, and the sign is negative (antiparallel) if gamma is positive.

4. Conclusions

Through a series of experiments, we have explored the relationship between the configuration of external magnetic field and laser Poynting vector for optical pumping. In this study, we have verified the mechanism invoked to describe the OPNMR phenomenon in GaAs, and have now demonstrated its applicability in CdTe. Such a comparison was possible by approaching these materials in an unambigious manner: the experimental configuration, the conventions for defining angular momentum in photons/electrons/nuclei, and the conventions used to phase the NMR spectra were carefully accounted for.

In GaAs, the OPNMR profiles have been reported before without a systematic accounting for the external magnetic field with respect to the laser. We have demonstrated the validity of spin

polarization by flipping the orientation of the external magnetic field, showing that the OPNMR profiles can be treated by considering the optical pumping selection rules. The "inversion" of the effects of the two circular polarizations between configurations is a consequence of angular momentum conventions. A hallmark of OPNMR is asymmetric signals arising from optical pumping for the two circular polarizations, which is attributed to the optical Overhauser effect (OE). The invariant negative optical OE observed in both configurations is consistent with an electron thermalization effect with a negative electron g^*.

In CdTe, the profiles are entirely positive in intensity for all photon energies studied here. CdTe, like GaAs, has a negative electron g^*, but the optical OE is positive in both experimental configurations. We show that this apparent positive optical OE is a consequence of how (OP) NMR signals are conventionally phased—phase does not directly impart knowledge of the sign of polarization. Rather, phase depends on both the sign of polarization as well as the sign of the nuclear gyromagnetic ratio. In CdTe, all NMR-active nuclei have negative gyromagnetic ratios, whereas in GaAs, all are positive. We connect the differences in signs of the gyromagnetic ratios to the apparent sign differences in the optical OE for both semiconductor systems.

In summary, the experimental configuration of $\boldsymbol{B}_0$ with respect to the Poynting vector of the laser, and the treatment of signal phase is an important aspect of optical pumping and NMR detection. Experiments should report the direction of $\boldsymbol{B}_0$ and phasing criteria in an effort to ensure reproducibility and accurate interpretation of spin hyperpolarization.

Declaration of Competing Interest

The authors declare that they have no known competing financial interests or personal relationships that could have appeared to influence the work reported in this paper.

Acknowledgments

This material is based upon work supported by the National Science Foundation under Grant No. (DMR-2004915). In addition, a portion of this work was performed by ELS, MMW, DDW, and ZM supported by the National Science Foundation under Grant No. (DMR- 1206447).

References

[1] M. Wu, Z. Li, T. Cao, S.G. Louie, Physical origin of giant excitonic and magneto-optical responses in two-dimensional ferromagnetic insulators, Nat. Commun. 10 (2019) 1.
[2] T. Haider, A review of magneto-optic effects and its application, Int. J. Electromagn. Appl. 7 (2017) 17.
[3] F. Dolde, V. Bergholm, Y. Wang, I. Jakobi, B. Naydenov, S. Pezzagna, J. Meijer, F. Jelezko, P. Neumann, T. Schulte-Herbrüggen, et al., High-fidelity spin entanglement using optimal control, Nat. Commun. 5 (2014) 1.
[4] J.A. Reimer, Nuclear hyperpolarization in solids and the prospects for nuclear spintronics, Solid State Nucl. Magn. Reson. 37 (2010) 3.
[5] D.P. DiVincenzo, The physical implementation of quantum computation, Fortschritte der Physik: Progress of Physics 48 (2000) 771.
[6] D. Loss, D.P. DiVincenzo, Quantum computation with quantum dots, Phys. Rev. A 57 (1998) 120.
[7] R. Hanson, D.D. Awschalom, Coherent manipulation of single spins in semiconductors, Nature 453 (2008) 1043.
[8] R. Blatt, C.F. Roos, Quantum simulations with trapped ions, Nat. Phys. 8 (2012) 277.
[9] J.I. Cirac, P. Zoller, Quantum computations with cold trapped ions, Phys. Rev. Lett. 74 (1995) 4091.
[10] C.D. Bruzewicz, J. Chiaverini, R. McConnell, J.M. Sage, Trapped-ion quantum computing: Progress and challenges, Appl. Phys. Rev. 6 (2019) 021314.
[11] K.C. Nowack, F.H.L. Koppens, Y.V. Nazarov, L.M.K. Vandersypen, Coherent control of a single electron spin with electric fields, Science 318 (2007) 1430.
[12] B.E. Kane, A silicon-based nuclear spin quantum computer, Nature 393 (1998) 133.
[13] T.D. Ladd, J.R. Goldman, F. Yamaguchi, Y. Yamamoto, E. Abe, K.M. Itoh, All-silicon quantum computer, Phys. Rev. Lett. 89 (2002) 017901.
[14] A. Goto, S. Ohki, K. Hashi, T. Shimizu, Optical switching of nuclear spin-spin couplings in semiconductors, Nat. Commun. 2 (2011) 375.
[15] T. Shimizu, A. Goto, K. Hashi, S. Ohki, An NMR quantum computer of the semiconductor CdTe, Superlatt. Microstruct. 32 (2002) 313.
[16] M. Kroutvar, Y. Ducommun, D. Heiss, M. Bichler, D. Schuh, G. Abstreiter, J.J. Finley, Optically programmable electron spin memory using semiconductor quantum dots, Nature 432 (2004) 81.
[17] J.R. Petta, A.C. Johnson, J.M. Taylor, E.A. Laird, A. Yacoby, M.D. Lukin, C.M. Marcus, M.P. Hanson, A.C. Gossard, Coherent manipulation of coupled electron spins in semiconductor quantum dots, Science 309 (2005) 2180.
[18] C. Kloeffel, D. Loss, Prospects for spin-based quantum computing in quantum dots, Annu. Rev. Condensed Matter Phys. 4 (2013) 51.
[19] T.P.M. Alegre, C. Santori, G. Medeiros-Ribeiro, R.G. Beausoleil, Polarization-selective excitation of nitrogen vacancy centers in diamond, Phys. Rev. B 76 (2007) 165205.
[20] F. Jelezko, J. Wrachtrup, Single defect centres in diamond: A review, Phys. Status Solidi A 203 (2006) 3207.
[21] L. Rondin, J.-P. Tetienne, T. Hingant, J.-F. Roch, P. Maletinsky, V. Jacques, Magnetometry with nitrogen-vacancy defects in diamond, Rep. Prog. Phys. 77 (2014) 056503.
[22] M. Dyakonov, V. Perel, Optical Orientation, Vol. 8 (North-Holland Physics Publishing, 1984) pp. 15–71.
[23] R. Tycko, J.A. Reimer, Optical pumping in solid state nuclear magnetic resonance, J. Phys. Chem. 100 (1996) 13240.
[24] S.E. Hayes, S. Mui, K. Ramaswamy, Optically pumped nuclear magnetic resonance of semiconductors, J. Chem. Phys. 128 (2008) 052203.
[25] D.D. Wheeler, M.M. Willmering, E.L. Sesti, X. Pan, D. Saha, C.J. Stanton, S.E. Hayes, Modelling of OPNMR phenomena using photon energy-dependent $\langle S_z \rangle$ in GaAs and InP, J. Magn. Reson. 273 (2016) 19.
[26] K. Ramaswamy, S. Mui, S.A. Crooker, X. Pan, G.D. Sanders, C.J. Stanton, S.E. Hayes, Optically pumped NMR: Revealing spin-dependent Landau level transitions in GaAs, Phys. Rev. B 82 (2010) 085209.
[27] R. Benumof, Optical pumping theory and experiments, Am. J. Phys. 33 (1965) 151.
[28] R.L. de Zafra, Optical Pumping, Am. J. Phys. 28 (1960) 646.
[29] H.G. Dehmelt, Slow spin relaxation of optically polarized sodium atoms, Phys. Rev. 105 (1957) 1487.
[30] A. Kastler, Optical methods of atomic orientation and of magnetic resonance, J. Opt. Soc. Am. 47 (1957) 460.
[31] E. Togan, Y. Chu, A.S. Trifonov, L. Jiang, J. Maze, L. Childress, M.V.G. Dutt, A.S. Sørensen, P.R. Hemmer, A.S. Zibrov, et al., Quantum entanglement between an optical photon and a solid-state spin qubit, Nature 466 (2010) 730.
[32] M.H. Levitt, Spin Dynamics - Basics of Nuclear Magnetic Resonance, 2nd ed., Wiley, 2008.
[33] K. Ramaswamy, S. Mui, S.E. Hayes, Light-induced hyperfine ^{69}Ga shifts in semi-insulating GaAs observed by optically polarized NMR, Phys. Rev. B 74 (2006) 153201.
[34] S. Mui, K. Ramaswamy, S.E. Hayes, Effects of optical absorption on ^{71}Ga optically polarized NMR in semi-insulating GaAs: Measurements and simulations, Phys. Rev. B 75 (2007) 195207.
[35] S. Mui, K. Ramaswamy, S.E. Hayes, Physical insights from a penetration depth model of optically pumped NMR, J. Chem. Phys. 128 (2008) 052303.
[36] P.J. Coles, J.A. Reimer, Penetration depth model for optical alignment of nuclear spins in gaas, Phys. Rev. B 76 (2007) 174440.
[37] S. Mui, K. Ramaswamy, C.J. Stanton, S.A. Crooker, S.E. Hayes, Manifestation of Landau level effects in optically-pumped NMR of semi-insulating GaAs, PCCP 11 (2009) 7031.
[38] E.L. Sesti, D.D. Wheeler, S.E. Hayes, D. Saha, G.D. Sanders, C.J. Stanton, Assignments of transitions in optically-pumped NMR of GaAs/AlGaAs quantum wells on a bulk GaAs substrate, Phys. Rev. B 90 (2014) 125301.
[39] R.M. Wood, D. Saha, L.A. McCarthy, J.T. Tokarski, G.D. Sanders, P.L. Kuhns, S.A. McGill, A.P. Reyes, J.L. Reno, C.J. Stanton, et al., Effects of strain and quantum confinement in optically pumped nuclear magnetic resonance in GaAs: Interpretation guided by spin-dependent band structure calculations, Phys. Rev. B 90 (2014) 155317.
[40] M.M. Willmering, E.L. Sesti, S.E. Hayes, R.M. Wood, C.R. Bowers, S.K. Thapa, C.J. Stanton, A.P. Reyes, P. Kuhns, S. McGill, Probing the magnetic field dependence of the light hole transition in GaAs/AlGaAs quantum wells using optically pumped NMR, Phys. Rev. B 97 (2018) 075303.
[41] K.L. Sauer, C.A. Klug, J.B. Miller, J.P. Yesinowski, Optically pumped InP: Nuclear polarization from NMR frequency shifts, Phys. Rev. B 84 (2011) 085202.
[42] C.A. Michal, R. Tycko, Nuclear spin polarization transfer with a single radio-frequency field in optically pumped indium phosphide, Phys. Rev. Lett. 81 (1998) 3988.
[43] C.A. Michal, R. Tycko, Stray-field NMR imaging and wavelength dependence of optically pumped nuclear spin polarization in InP, Phys. Rev. B 60 (1999) 8672.
[44] A. Goto, K. Hashi, T. Shimizu, R. Miyabe, X. Wen, S. Ohki, S. Machida, T. Iijima, G. Kido, Optical pumping NMR in the compensated semiconductor InP:Fe, Phys. Rev. B 69 (2004) 075215.
[45] A.K. Paravastu, S.E. Hayes, B.E. Schwickert, L.N. Dinh, M. Balooch, J.A. Reimer, Optical polarization of nuclear spins in GaAs, Phys. Rev. B 69 (2004) 75203.
[46] S.E. Barrett, R. Tycko, L.N. Pfeiffer, K.W. West, Directly detected nuclear magnetic resonance of optically pumped GaAs quantum wells, Phys. Rev. Lett. 72 (1994) 1368.

[47] A. Goto, K. Hashi, S. Ohki, T. Shimizu, Interface-sensitive nuclear magnetic resonance at a semiconductor heterojunction using hyperpolarization, Phys. Rev. Mater. 1 (2017) 074601.
[48] C.R. Bowers, Microscopic interpretation of optically pumped NMR signals in GaAs, Solid State Nucl. Magn. Reson. 11 (1998) 11.
[49] A. Abragam, The Principles of Nuclear Magnetism, 32, Oxford University Press, 1961.
[50] G. Kaur, G. Denninger, Dynamic nuclear polarization in III–V semiconductors, Appl. Magn. Reson. 39 (2010) 185.
[51] C. Weisbuch, C. Hermann, Optical detection of conduction-electron spin resonance in GaAs, $Ga_{1-x}In_xAs$, and $Ga_{1-x}Al_xAs$, Phys. Rev. B 15 (1977) 816.
[52] L.M. Roth, B. Lax, S. Zwerdling, Theory of optical magneto-absorption effects in semiconductors, Phys. Rev. 114 (1959) 90.
[53] A.M. White, I. Hinchliffe, P.J. Dean, P.D. Greene, Zeeman spectra of the principal bound exciton in sn-doped gallium arsenide, Solid State Commun. 10 (1972) 497.
[54] G. Lampel, Nuclear dynamic polarization by optical electronic saturation and optical pumping in semiconductors, Phys. Rev. Lett. 20 (1968) 491.
[55] P.L. Kuhns, A. Kleinhammes, T. Schmiedel, W.G. Moulton, P. Chabrier, S. Sloan, E. Hughes, C.R. Bowers, Magnetic-field dependence of the optical Overhauser effect in GaAs, Phys. Rev. B 55 (1997) 7824.
[56] I.J.H. Leung, C.A. Michal, Optical enhancement of NMR signals in CdTe, Phys. Rev. B 70 (2004) 035213.
[57] T. Pietraß, A. Bifone, T. Rõõm, E.L. Hahn, Optically enhanced high-field NMR of GaAs, Phys. Rev. B 53 (1996) 4428.
[58] R. Tycko, Optical pumping in indium phosphide: 31P NMR measurements and potential for signal enhancement in biological solid state NMR, Solid State Nucl. Magn. Reson. 11 (1998) 1.
[59] D. Paget, G. Lampel, B. Sapoval, V.I. Safarov, Low field electron-nuclear spin coupling in gallium arsenide under optical pumping conditions, Phys. Rev. B 15 (1977) 5780.
[60] D. Paget, Optical detection of NMR in high-purity GaAs under optical pumping: Efficient spin-exchange averaging between electronic states, Phys. Rev. B 24 (1981) 3776.
[61] D. Paget, Optical detection of nmr in high-purity gaas: Direct study of the relaxation of nuclei close to shallow donors, Phys. Rev. B 25 (1982) 4444.
[62] M.J. Snelling, G.P. Flinn, A.S. Plaut, R.T. Harley, A.C. Tropper, R. Eccleston, C.C. Phillips, Magnetic g factor of electrons in gaas/al x ga 1–x as quantum wells, Physical Review B 44 (1991) 11345.
[63] A. Nakamura, D. Paget, C. Hermann, C. Weisbuch, G. Lampel, B.C. Cavenett, Optical detection of electron spin resonance in CdTe, Solid State Commun. 30 (1979) 411.